Towards a Statistical Atlas of Cardiac Fiber Architecture

Jean-Marc Peyrat, Maxime Sermesant, Hervé Delingette, Xavier Pennec, Chenyang Xu, Elliot R. Mcveigh, Nicholas Ayache

INSTITUT NATIONAL DE RECHERCHE EN INFORMATIQUE ET EN AUTOMATIQUE

Towards a Statistical Atlas of Cardiac Fiber Architecture

Jean-Marc Peyrat — Maxime Sermesant — Hervé Delingette — Xavier Pennec —

Chenyang Xu — Elliot McVeigh — Nicholas Ayache

N° 5906

April 2006

Thème BIO

ISSN 0249-6399 ISRN INRIA/RR--5908--FR+ENG

Towards a Statistical Atlas of Cardiac Fiber Architecture

Jean-Marc Peyrat* , Maxime Sermesant* , Hervé Delingette* , Xavier Pennec* , Chenyang Xu† , Elliot McVeigh‡ , Nicholas Ayache*

Thème BIO — Systèmes biologiques
Projets Asclepios

Rapport de recherche n° 5906 — April 2006 — 26 pages

Abstract: We propose here a framework to build a statistical atlas of diffusion tensors of canine hearts. The anatomical images of seven hearts are first non-rigidly registered in the same reference frame and their associated diffusion tensors are then transformed with a method that preserves the cardiac laminar sheets. In this referential frame, the mean tensor and its covariance matrix are computed based on the Log-Euclidean framework. With this method, we can produce a smooth mean tensor field that is suited for fiber tracking algorithms or the electromechanical modeling of the heart. In addition, by examining the covariance matrix at each voxel it is possible to assess the variability of the cardiac fiber directions and of the orientations of laminar sheets. The results show a strong coherence of the diffusion tensors and the fiber orientations among a population of seven normal canine hearts.

Key-words: DT-MRI, DTI, diffusion tensor, Log-Euclidean, cardiac fiber, heart, myocardium, atlas

* ASCLEPIOS Research Project - INRIA
† Siemens Corporate Research, Princeton, NJ, USA
‡ Laboratory of Cardiac Energetics, National Heart Lung and Blood Institute, Bethesda, Maryland, USA

Vers un Atlas Statistique de l'Architecture des Fibres Cardiaques

Résumé : Dans ce rapport, nous présentons un cadre pour construire un atlas statistique des tenseurs de diffusion de cœurs de chien. Tout d'abord les images anatomiques de sept cœurs sont recalées de manière non-rigide dans le même référentiel et leurs tenseurs de diffusion associés sont alors transformés suivant une méthode qui conserve les feuillets laminaires des fibers cardiaques. Dans ce référentiel, un tenseur moyen et sa matrice de covariance sont calculés avec la métrique Log-Euclidienne. Avec cette méthode, nous obtenons un champ de tenseurs moyens lisse qui convient à une reconstruction des fibers ou à une modélisation électromécanique du cœur. De plus, en examinant la matrice de covariance en chaque voxel il est possible d'évaluer la variabilité de la direction des fibres cardiaques et de l'orientation des feuillets laminaires. Les résultats montrent une grande cohérence des tenseurs de diffusion et des orientations des fibres dans une population de sept cœurs normaux de chiens.

Mots-clés : DT-MRI, DTI, tenseur de diffusion, Log-Euclidien, fibre cardiaque, cœur, myocarde, atlas

Contents

1 Introduction

While the main geometrical arrangement of myofibers has been known for decades, its variability between subjects and species still remains largely unknown. Understanding this variability is not only important for a better description of physiological principles but also for the planning of patient-specific cardiac therapies [22]. Furthermore, the knowledge of the relation between the myocardium shape and its myofiber architecture is an important and required stage towards the construction of computational models of the heart [4] [19] since the fiber orientation plays a key role when simulating the electrical and mechanical function of the heart.

The knowledge about fiber orientation has been recently eased with the use of Diffusion Tensor Imaging (DTI) since there is a correlation between the myocardium fiber structure and diffusion tensors [13] [21]. DTI also has the advantage to provide directly this information in 3D with a high resolution but it is unfortunately not available *in vivo* due to the cardiac motion. There has been several works [7] [11] [12] in the past decade that have studied the variability of fiber orientation from DTI (similar studies has been done for brain as well [14]). Those studies estimated the fiber direction as the first eigenvector of each tensor and for instance compared its transmural variation with that observed from dissection experiments.

We propose here to extend those studies by building a statistical model of the whole diffusion tensor and not only its first eigenvector. This tensor analysis allows us to study the variability of laminar sheets which are associated with the second and third eigenvectors. Performing this analysis based on vector analysis (instead of tensor analysis) would have been difficult because the second and third eigenvalues have often very similar values and may lead to interpretation errors. To the best of our knowledge, this is the first attempt to perform a first and second order statistical analysis of DT images of canine hearts.

Our statistical analysis proceeds as follows. We first register the seven canine heart images in a same reference frame using anatomical MR images. Then we properly transform the diffusion tensors considering properties of the cardiac fiber microstructure. Finally we use coherent statistical tools on tensors to study the variability of individual hearts from this average model and to evaluate the relevance of such a model. An application of this framework is done using a dataset of seven normal canine hearts.

2 Materials and Methods

2.1 Data Acquisition

We used a dataset of seven *ex vivo* perfused normal canine hearts acquired and provided by the Center of Cardiovascular Bioinformatics and Modeling (CCBM)[1] at the Johns Hopkins University. Each heart was placed in an acrylic container filled with Fomblin, a perfluoropolyether (Ausimon, Thorofare, NJ). Fomblin has a low dielectric effect and minimal MR signal thereby increasing contrast and eliminating unwanted susceptibility artifacts near the boundaries of the heart. The long axis of the hearts was aligned with the z-axis of the scanner. Images were acquired with a 4-element knee phased array coil on a $1.5T$ GE CV/I MRI Scanner (GE, Medical System, Wausheka, WI) using an enhanced gradient system with $40mT/m$ maximum gradient amplitude and a $150T/m/s$ slew rate. Different resolutions have been used around $0.3 \times 0.3 \times 0.9\ mm^3$ and from 14 to 28 gradient directions. The images have been subsampled into $128 \times 128 \times 64$ images with a resolution around $0.6 \times 0.6 \times 1.8\ mm^3$. The temperature during acquisition varied between $18 - 25\,^{\circ}\mathrm{C}$ from one heart to another.

A diffusion tensor T is a covariance matrix describing the anisotropic Brownian motion of water molecules. Its eigenvalue decomposition leads to $T = PDP^T$ with P the matrix of the eigenvectors V and D the diagonal matrix of the eigenvalues. The eigenvalues of the diffusion tensor quantifies the diffusion rate of water molecules within the tissue structure along the directions given by the corresponding eigenvectors. These eigenvalues are directly linked to the mean free path of water molecules.

2.2 Myocardium Registration

We register DT images based on anatomical MRIs since we want to compare the diffusion tensors corresponding to anatomical regions of different hearts without any prior knowledge on their statistical variability. We would have introduced a bias in DTI analysis using DTI registration algorithms [9] [24] [18] or fiber direction registration [7]. Before the registration stage, we pre-process semi-automatically the images by extracting the image background, and by cropping each image above the valve plane. We register the hearts on a template given by an iterative mean estimation. It means we register each MR image onto a chosen one from the dataset and once we have a first set of registered MRIs, we compute its mean image that is used as a template for the next iteration. These iterations should be repeated until convergence but usually one or two iterations are sufficient to get a good approximation of the expected mean. The registration algorithm is initialized with a global affine transformation of the hearts (cf. Section A.1 for more details about the global affine transformation we used) in order to ease the second non-rigid registration step. This second registration step is based on a hybrid non-rigid intensity- and landmark-based registration algorithm [5]. The hybrid algorithm gives us the ability to interactively refine the registration of a local region.

[1] http://www.ccbm.jhu.edu/research/DTMRIDS.php

The output of this process is a dense deformation field for each anatomically registered cardiac image.

2.3 Transformation of Cardiac Diffusion Tensors

The next stage is to transform the DT image based on the estimated deformation field. For each voxel, the global deformation field is approximated at the first order by an affine transformation. This underlying affine transformation A is computed from the identity matrix Id and the Jacobian ∇F of the deformation field F (computed with a 3D Sobel-filter):

$$A = Id + \nabla F$$

Now we have the well known problem of applying an affine transformation to a diffusion tensor image. Since it was shown that there is a correlation between the cardiac tissue microstructure and the eigensystem of the diffusion tensors [12] [13] [21], we can transform the underlying tissue microstructure with the affine transformation. Then we reconstitute the diffusion tensor from this transformed microstructure knowing the relationship between the two of them. The solution we propose here to handle this problem proved to be similar to the *Preservation of the Principal Direction* (PPD) reorientation strategy [1]:

$$V_1' = \frac{AV_1}{||AV_1||} \qquad V_3' = \frac{(A^{-1})^T V_3}{||(A^{-1})^T V_3||} \qquad V_2' = V_3 \otimes V_1$$

where V_1, V_2, V_3 are the primary, secondary and tertiary eigenvectors of the original diffusion tensor and where V_1', V_2', V_3' are the ones of the transformed diffusion tensor.

The PPD has been already justified and validated in the case of brain DTI [1] but only partially in the case of cardiac DTI. We propose here a more complete justification of the PPD strategy for cardiac DTI transformation.

As described in Figure 1, the myocardium microstructure is made of laminar sheets of muscle fibers [16]. The space between the laminar sheets is composed of extracellular water and collagen network linking these sheets together. This extracellular space has a mostly unrestricted diffusion in the direction of the first two eigenvectors of the diffusion tensor. The interface plane between the laminar sheets and the extracellular space is an important barrier for water molecules and its normal defines the third eigenvector. The extracellular water between fibers in the laminar planes can explain the difference between the primary eigenvector in the fiber direction and the secondary eigenvector orthogonal to the fiber direction. But the cardiomyocyte geometry is also proposed to explain the privileged diffusion direction in the fiber orientation. A cardiomyocyte is much longer (50-120 μm) than wider (5-25 μm) and much longer than the mean free path (roughly 10 μm in our case). It means that the cell membrane does not have an important influence on the water diffusion in the fiber direction. Nevertheless the mean free path is still lower than the one in an unrestricted diffusivity region because of the subcellular structures as organelles,

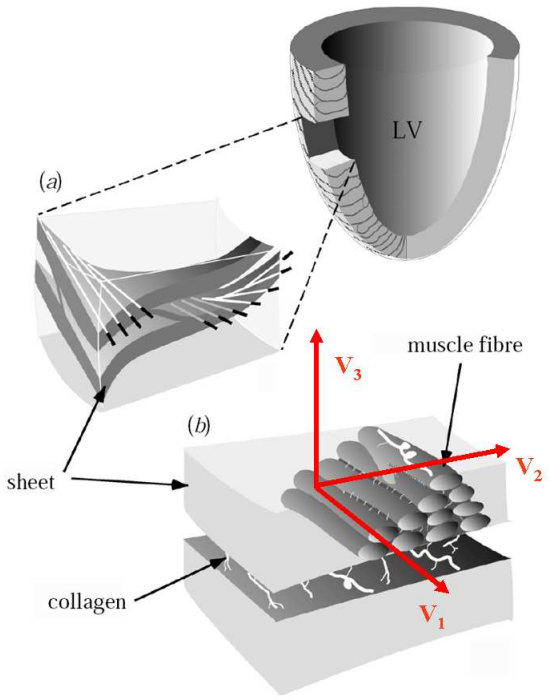

Figure 1: From the macrostructure to the microstructure of cardiac fibers (from LeGrice *et al.* [16]). Link between the primary eigenvector V_1, the secondary eigenvector V_2 and the tertiary eigenvecor V_3 of the diffusion tensor and the underlying structure.

structural proteins, myofilaments, etc. This is not the case in the other directions where the width of the cells is close to the mean free path.

Let us now analyze the effect of the basic transformations (translations, rotations, shears and scaling) describing an affine transformation. The way to transform the fiber structure and thus the diffusion tensors through translation and rotation is obvious. The scaling only changes the density of fibers microstructure inside a voxel (we consider that the cells size and the thickness of the laminar sheets and intralaminar spaces are roughly the same in all hearts) and finally not the diffusion rate *i.e.* the eigenvalues of the diffusion tensor. The shearing induced by the affine transformation is not so simple to apply to the diffusion tensors. We illustrate in Figure 2 the shearing applied to the basic microstructure of cardiac fibers. The direct transformation of the original eigenvectors V_i leads to the vector AV_i and the transformation deduced from the fiber structure deformation leads to the vector V_i'. As we determine the fiber structure deformation through the fiber direction deformation, the

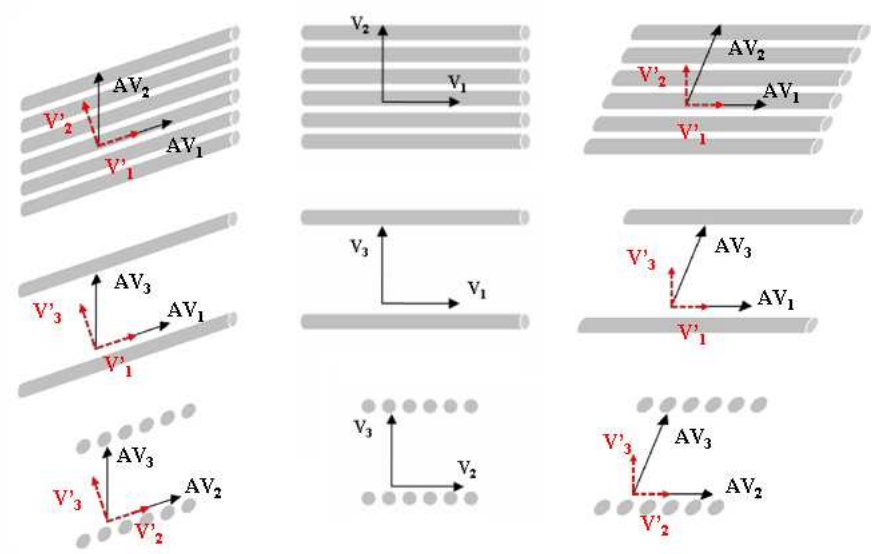

Figure 2: [*Middle*] Original basic fiber microstructure with eigenvectors V_i [*Left and Right*] Shearing applied to the basic fiber microstructure : continuous arrows AV_i are the transformed eigenvectors through the shearing and dashed arrows V_i' are the eigenvectors regarding to the correlation between the fiber microstructure and the diffusion tensor.

transformed primary eigenvector V_1' is the same as the direct transformation of the original primary eigenvector V_1:

$$V_1' = \frac{AV_1}{||AV_1||}$$

The tertiary eigenvector is defined by n, the vector normal to the laminar sheets which are considered locally plane. The image of a plane through an affine transformation is a plane. It means that these laminar sheets are stable. We just have to find n' the unit vector normal to the plane defined by the image V_1' of V_1 and the image AV_2 of V_2 [23]:

$$n' = \frac{(A^{-1})^T n}{||(A^{-1})^T n||}$$

The transformed secondary eigenvector obtained from the correlation between the structure of the fibers happens to be the one that builds an orthonormal basis with the two others. It means that constructing first the secondary (as done for the PPD) or the tertiary (as we do) and then determine the other one to obtain an orthonormal basis leads to the same results. This is the keypoint that justifies the use of the PPD in our specific case of cardiac DTI. A more complex structure with crossing fibers is a good counter-example where

this strategy is not optimal, it would lead to a simplification of the underlying structure deformation.

2.4 Tensor Statistics

2.4.1 Log-Euclidean Mean and Covariance Computation

The Log-Euclidean framework [2] provides a consistent and rigorous framework to study the statistical variability of DTI for each voxel of the heart. In this framework the space of diffusion tensors is a vectorial space which means it inherits from all the statistical properties and tools we can get from a vectorial space. We thus compute the mean of all the registered DTI and the corresponding covariance [17] at each voxel:

$$\overline{D}_{log} = \exp(\frac{1}{N}\sum_{i=1}^{N}\log(D_i))$$

$$Cov = \frac{1}{N-1}\sum_{i=1}^{N} vect(\log(D_i) - \log(\overline{D}_{log})).vect(\log(D_i) - \log(\overline{D}_{log}))^T$$

where $vect(D)$ is the vectorial representation [17] of the diffusion tensor D.

2.4.2 Log-Euclidean Covariance Analysis

The difficulty to visualize the 6×6 covariance matrix of diffusion tensors leads us to study first its norm $\sqrt{Trace(Cov)}$, which allows us to identify the variable and stable regions of the heart. To help us in translating the DTI variability into the fiber structure variability, we can analyze this covariance matrix extracting 6 specific variance parameters at each voxel in the coordinate system of the mean tensor: 3 for each eigenvalue variability and the 3 for each eigenvectors orientation variability around the mean.

Let us consider the diagonalization of the mean in the Log-Euclidean space:

$$\overline{W} = \log(\overline{D}_{log}) = \sum_{i=1}^{3} \lambda_i V_i {V_i}^T$$

where $\lambda_i = \log d_i$ and d_i are the eigenvalues of the diffusion tensor $\overline{D}_{log}$

Considering small variations $\delta\lambda_i$ and δV_i of the eigenvalues λ_i and the orthonormal eigenvectors V_i around the mean diffusion tensor:

$$\overline{W} + \delta W = (\lambda_1 + \delta\lambda_1)(V_1 + \delta V_1)(V_1 + \delta V_1)^T + (\lambda_2 + \delta\lambda_2)(V_2 + \delta V_2)(V_2 + \delta V_2)^T + (\lambda_3 + \delta\lambda_3)(V_3 + \delta V_3)(V_3 + \delta V_3)^T$$

$$\text{where } \delta V_1 = \epsilon_{12}V_2 + \epsilon_{13}V_3,\ \delta V_2 = \epsilon_{21}V_1 + \epsilon_{23}V_3 \text{ and } \delta V_3 = \epsilon_{31}V_1 + \epsilon_{32}V_2$$

Since V_1,V_2 and V_3 build an orthonormal basis of $\mathbb{R}^3$: $\epsilon_{ij} = -\epsilon_{ji}$. Finally considering only the first order terms leads to:

$$\delta W = \sum_{i=1}^{3} \delta\lambda_i W_i + \sqrt{2}(\lambda_2 - \lambda_3)\epsilon_{23} W_4 + \sqrt{2}(\lambda_1 - \lambda_3)\epsilon_{13} W_5 + \sqrt{2}(\lambda_1 - \lambda_2)\epsilon_{12} W_6$$

where the W_i form an orthonormal basis of the tangent space at the mean diffusion tensors:

$$W_1 = V_1 {V_1}^T \qquad W_4 = \frac{1}{\sqrt{2}}(V_3 {V_2}^T + V_2 {V_3}^T)$$
$$W_2 = V_2 {V_2}^T \qquad W_5 = \frac{1}{\sqrt{2}}(V_3 {V_1}^T + V_1 {V_3}^T)$$
$$W_3 = V_3 {V_3}^T \qquad W_6 = \frac{1}{\sqrt{2}}(V_2 {V_1}^T + V_1 {V_2}^T)$$

Eigenvalues Variability The projections of the covariance on the W_1, W_2 and W_3 vectors describe the variances of the three eigenvalues in the Log-Euclidean space.

$$E({\delta\lambda_i}^2) = vect(W_i)^T.Cov.vect(W_i) \qquad i = 1, 2, 3$$

We can directly study the variability of the original diffusion tensor eigenvalues in the Euclidean space using the following relationship: $\lambda_i = \log(d_i) \Rightarrow \delta\lambda_i = \frac{\delta d_i}{d_i}$

$$E({\delta d_i}^2) = {d_i}^2[E({\delta\lambda_i}^2)] = {d_i}^2[vect(W_i)^T.Cov.vect(W_i)] \qquad i = 1, 2, 3$$

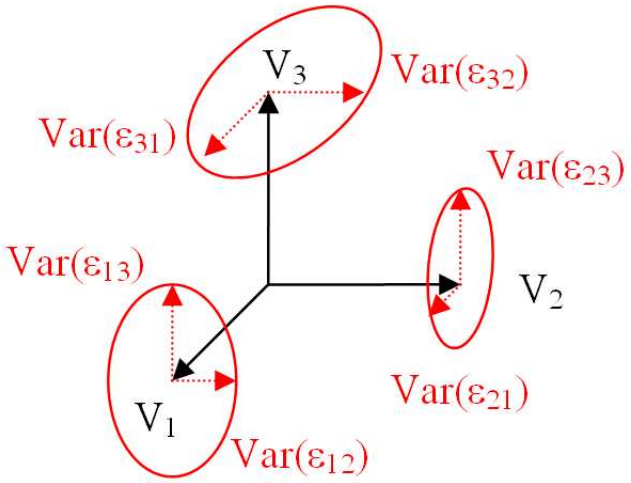

Figure 3: Orientation variability of eigenvectors

These variances $E(\delta\lambda_i{}^2)$ are also interesting to study directly since they can be linked to the normalized scatter measure of the diffusion tensors about their mean [14]. Indeed, the normalized scatter measure $\overline{S}_2$ describes a global dispersion of all the eigenvalues at the same time:

$$\overline{S}_2{}^2 = \frac{\frac{1}{N-1}\sum_{i=1}^{N}\|D_i - \overline{D}\|^2}{\|\overline{D}\|^2} = \frac{E(\|\delta D\|^2)}{\|\overline{D}\|^2} = \frac{\sum_{i=1}^{3} E(\delta d_i{}^2)}{\sum_{i=1}^{3}\overline{d}_i{}^2}$$

By contrast, the standard deviation of the eigenvalues in the Log-Euclidean space extracted from the covariance matrix gives information on the normalized dispersion of each eigenvalues about its Log-Euclidean mean *independently*:

$$E(\delta\lambda_i{}^2) = \frac{E(\delta d_i{}^2)}{\overline{d}_i{}^2} \qquad i = 1,2,3$$

Eigenvectors Orientation Variability Let us consider now the orientation variability of these eigenvectors. The projections on W_4, W_5 and W_6 represent the rotation of the coupled orthonormal vectors (V_2, V_3), (V_1, V_3) and (V_2, V_3) respectively around V_1, V_2 and V_3 (cf. Figure 3).

$$\begin{aligned}
Var(\epsilon_{23}) = E(\epsilon_{23}{}^2) &= \frac{1}{2(\lambda_2-\lambda_3)^2}[vect(W_4)^T.Cov.vect(W_4)] \\
Var(\epsilon_{13}) = E(\epsilon_{13}{}^2) &= \frac{1}{2(\lambda_1-\lambda_3)^2}[vect(W_5)^T.Cov.vect(W_5)] \\
Var(\epsilon_{12}) = E(\epsilon_{12}{}^2) &= \frac{1}{2(\lambda_1-\lambda_2)^2}[vect(W_6)^T.Cov.vect(W_6)]
\end{aligned}$$

It is important to notice that the rotation variability is highly dependent on the accuracy of the distinction between primary, secondary and tertiary eigenvectors. Indeed if two eigenvalues are similar the diffusion tensor describes an isotropic plane from which the extraction of eigenvectors has a lack of relevancy in terms of structural meaning. An isotropic plane can be defined by any orthonormal basis of vectors contained in this plane.

The dyadic coherence has already been proposed [6] [14] to assess the orientation dispersion about the mean direction. The dyadic coherence κ is defined as:

$$\kappa = 1 - \sqrt{\frac{\beta_2+\beta_3}{2\beta_1}}$$

where β_i are the eigenvalues of the mean dyadic tensor $\overline{V.V^T}$ of the diffusion eigenvector V at each voxel sorted from the largest to the smallest $(i = 1,2,3)$.

As we are working on unit vectors [8]:

$$\beta_1 + \beta_2 + \beta_3 = 1$$

which means $\beta_1 = 1 - (\beta_2 + \beta_3) = 1 - \sigma^2$.

The dyadic coherence $\kappa = 1 - \sqrt{\frac{\sigma^2}{2(1-\sigma^2)}}$ is linked to the radius of the cone of uncertainty around the eigenvector V. In the same way, that normalized scatter value of $\overline{S}_2$ describes a global dispersion of the eigenvalues, the dyadic coherence describes a global dispersion of the eigenvectors orientation where we can extract a dispersion of the eigenvectors orientation from the covariance matrix in a specific direction Thus we have access to an ellipsoidal cone of uncertainty (cf. Figure 3) around the eigenvector instead of a circular one with the dyadic coherence.

Finally the covariance matrix analysis has the advantage to provide less global and more accurate information about the variabilities of the eigenvectors and eigenvalues of the diffusion tensor, as well as the variability of the diffusion tensor itself without distinguishing eigenvalues and eigenvectors.

3 Results

We applied the proposed framework to the dataset of seven canine hearts presented previously. We obtain a smooth average cardiac DTI (cf. Figure 4 and 5) catching the shared transmural variation of the fibers directions (cf. Figure 4) that is similar to the one generally observed [20]. The norm of the covariance matrix in Figure 6 shows a global stability of the compact myocardium and several variable regions especially at the RV and LV endocardial apices where the fiber structure is probably less organized. Some other variabilities at the surface of the heart might also be due to registration artifacts.

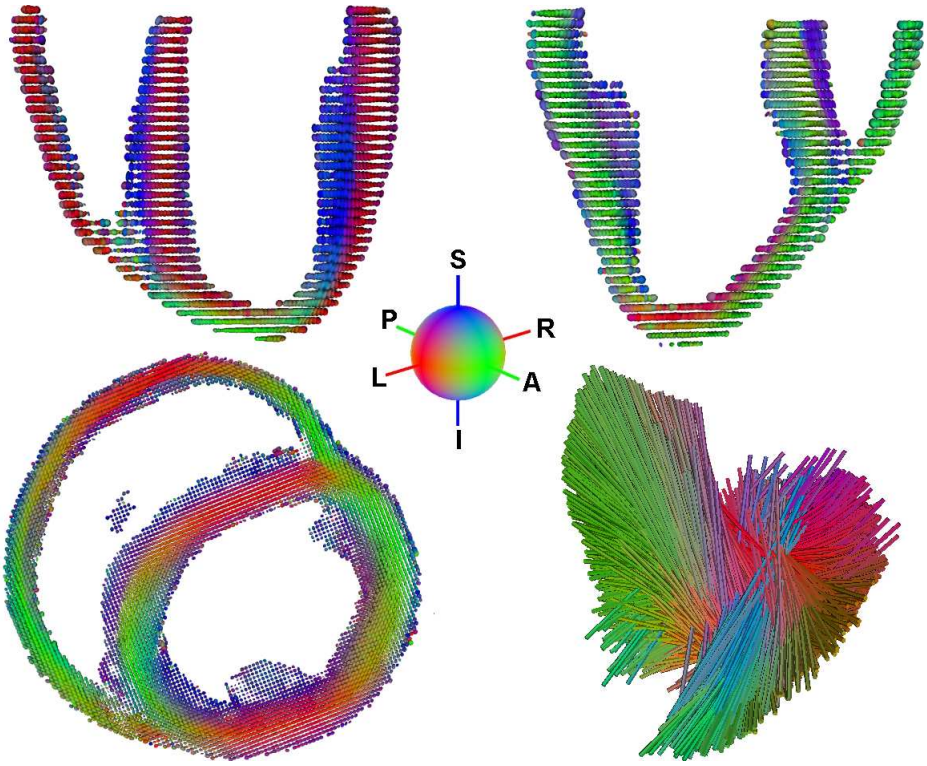

Figure 4: [*Left and Upper Right*] Average Canine Cardiac DTI showing smooth directions [*Lower Right*] Fiber tracking in the left ventricle wall with high stiffness parameters for a better visualization of the fan cardiac architecture varying with the transmural depth. In all the figures the RGB colors represent the components of the primary eigenvector $Red = |V_x|$, $Green = |V_y|$, $Blue = |V_z|$ with x, y in the axial plane and z orthogonal to the axial plane as described with the colored sphere.

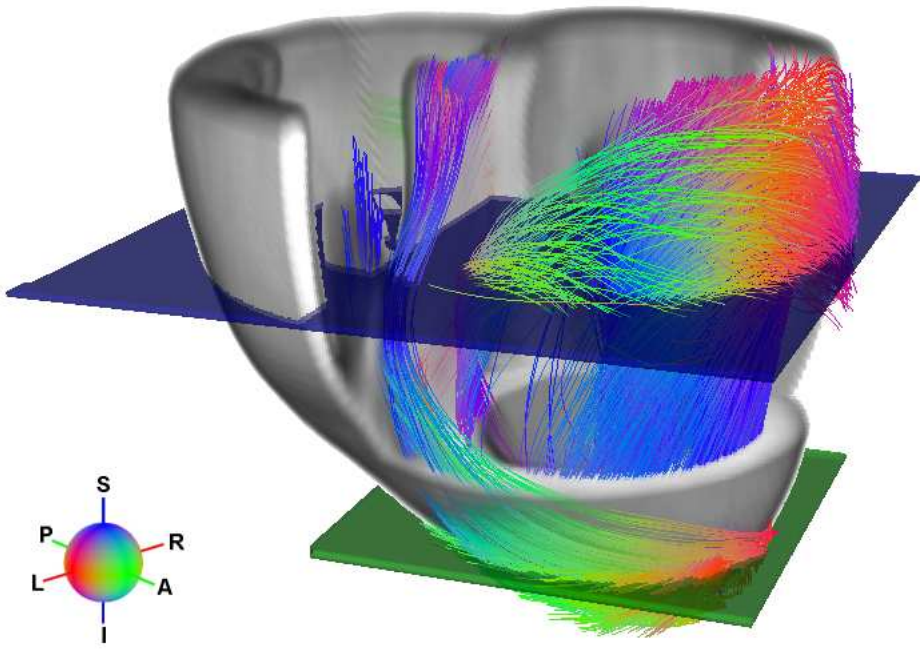

Figure 5: Fiber tracking on the average cardiac DTI. The fibers displayed cross the two planes in blue and green.

In order to have a better interpretation of this covariance matrix and to understand the origin of the variabilities, we decompose it into specific modes as described previously. We can see in Figures 6 that the eigenvalues variabilities are homogeneous in the compact myocardium. There are still some differences in the variability between eigenvalues but considering their variability proportionally to their mean value, we expect a significant variability of their fractional anisotropy (cf. Figure 7). Knowing that the temperature acquisition was not the same for all the hearts ($18 - 20\,^{\circ}\mathrm{C}$ and $25\,^{\circ}\mathrm{C}$), the variability of the eigenvalues might not be so relevant to study. Mostly the order of the eigenvalues is important. Indeed even if we introduce these values in an electromechanical model we do not really know how to translate them in terms of electrical conductivity [20]. The ongoing work on the development of current density imaging techniques [15] could help in determining such a correlation. The statistical study of these eigenvalues gives us an idea of the average values of diffusion which are uniformly distributed in each heart and uniformly variable among the population of hearts. At least, it could help in detecting locally defined pathologies.

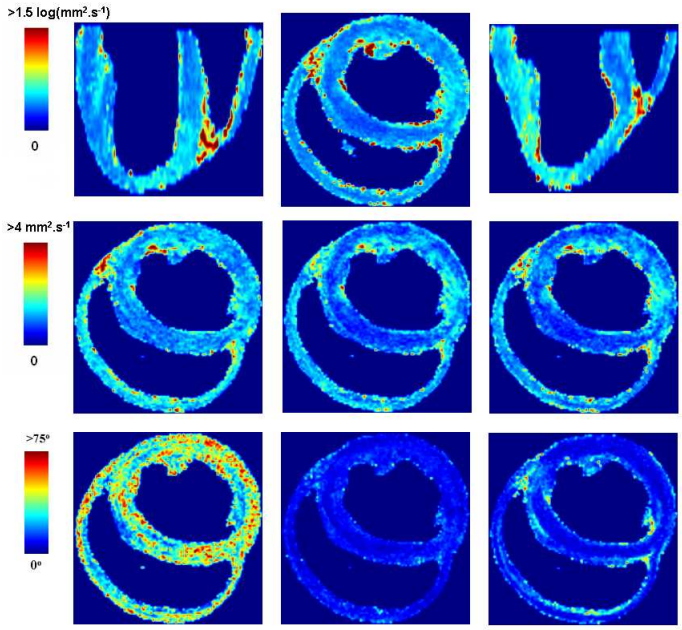

Figure 6: Statistical Variability of Diffusion Tensors. Norm of the covariance matrix (*upper in 3 orthogonal views* - more figures in Section A.2). Decomposition of the covariance in 6 eigenmodes describing the variability of the 1^{st}, 2^{nd}, 3^{rd} eigenvalues (*from middle left to middle right*) and the rotation of the plane orthogonal to the 1^{st}, 2^{nd} and 3^{rd} eigenvectors (*from lower left to lower right*).

The separation of the eigenvalues variability and the eigenvectors orientation variability is important to evaluate the variability of the myocardial fibers architecture. As seen in Figures 6 (and in Figures 10 and 11 in Section A.2), the orientation of the fibers is stable among a population (mean standard deviation of 8.8 and 9.4 degrees around the secondary and the tertiary eigenvectors) for the two rotations in the planes containing the primary eigenvector. It means that the fiber orientation of the average cardiac DTI is shared by the dataset. The orientation of the laminar sheets described by the rotation of the plane $Span(V_2, V_3)$ around V_1 shows a much higher mean standard deviation of 23 degrees. First of all this variability is underevaluated considering that the statistical study we proposed is a simplification at the first order. Secondly this variability is due to the difficulty to differentiate the secondary and tertiary eigenvectors when they have similar eigenvalues. When we study the fiber organization (i.e. the 3 rotation eigenmodes) we are not anymore in the diffusion tensor space and an isotropic plane of diffusion leads to a low accuracy in translating it into structural information. To achieve it an additionnal information will

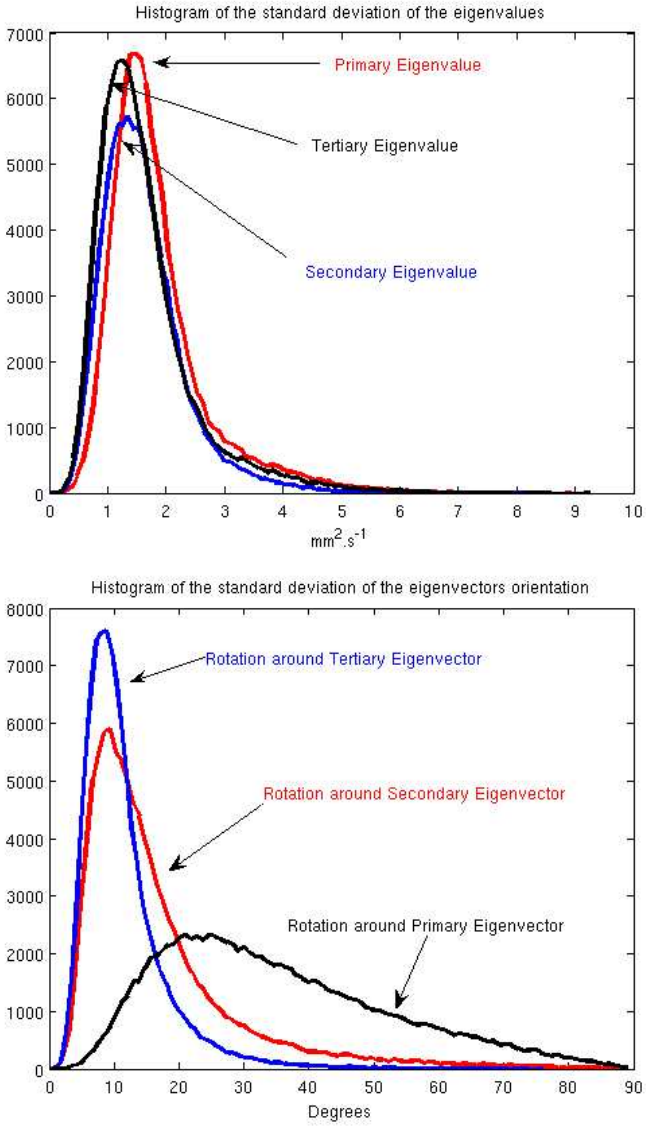

Figure 7: Spatial Histogram (number of voxels) of the standard deviation of the 6 eigenmodes: $E(\epsilon_{12}^2)$, $E(\epsilon_{23}^2)$, $E(\epsilon_{13}^2)$, $E(\delta {d_1}^2)$, $E(\delta {d_2}^2)$ and $E(\delta {d_3}^2)$. A standard deviation is computed at each voxel from the set of seven registered normal canine hearts.

be necessary as the one coming from the neighbourhood [11]. Another explanation might also be the existence of two populations of symmetric laminar sheets organization in canine hearts [11] [12] (and ovine hearts [10] as well) corresponding to the optimal configurations to maximize the systolic shear [3]. Mixing these two populations leads to the computation of an average cardiac DTI model that does not represent a real case of laminar sheets organization. The clustering of these populations will be necessary to confirm this hypothesis and then to build two different models of cardiac fibers architecture. A computation of the normal of the laminar sheets (with a sheet tracking algorithm for example) and a further study of their orientation variability is essential to determine its origin and of course to translate an atlas of cardiac DTI into an atlas of the cardiac fiber architecture.

4 Conclusion

We proposed a theoretically grounded, simple and powerful framework working directly on diffusion tensors to build an average model and to study their variability over a population of cardiac DTIs. The use of these average models instead of analytical models is an important stage to refine the electromechanical modeling with more accurate and reliable data and also with additional informations concerning the anisotropy in the plane orthogonal to the fiber directions. This framework is a first step towards a statistical atlas of the cardiac fiber architecture that will probably lead to a better understanding of the cardiac fiber architecture shared by a population of healthy or failing hearts, or to compare and to differentiate populations of hearts (canine-human, normal-failing...).

The results presented were obtained from a dataset of seven canine hearts. A more important dataset of hearts is needed to get a statistically reliable atlas. Another step would be to apply this framework to human hearts in perspective of clinical applications.

5 Acknowledgments

Drs. Patrick A. Helm and Raimond L. Winslow at the Center for Cardiovascular Bioinformatics and Modeling for provision of data. Antoine Azar for his technical support concerning the registration part of the framework. Pierre Fillard for provision of diffusion tensors and fiber tracking computation and visualization tools [2]. I.J. LeGrice for provision of an illustration in Figure 1.

[2] http://www-sop.inria.fr/epidaure/personnel/Pierre.Fillard/softwares/

A Appendix

A.1 Details about the Registration Algorithm

Basically, the first registration step is an initialization for the non-rigid registration. Indeed, the non-rigid registration algorithm we use has been designed for small displacements. It can lead to unexpected results when large displacements are computed. To solve this problem, we propose here to apply first a global affine transformation A using specific landmarks that are easy to define and to identify geometrically: the RV and LV endocardial apices (A_{RV} and A_{LV}) and the 2 corner points of the right ventricle in the valve plane (C_1 and C_2). As long as these 4 landmarks do not lead to an ill-posed problem (which should be the case most of the time considering the heart geometry and the chosen landmarks), they define a unique global affine transformation. Otherwise more landmarks could be used for a robust least square estimation of the global affine transformation.

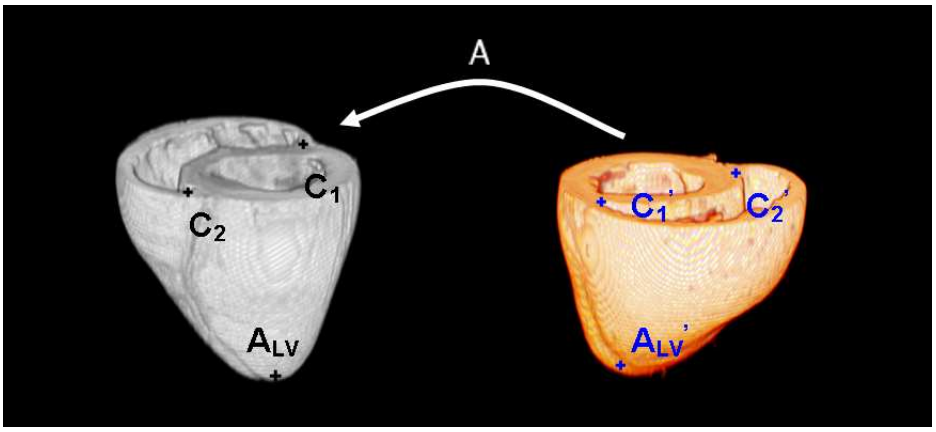

Figure 8: Initialization of the myocardium registration: global affine transformation A.

Actually, we currently use only 3 of these 4 landmarks (cf. Figure 8). The matching of the corner points defines (cf. Figures 9):

1. a rotation $R_{O_z,\theta}$ around the direction of the axis of the heart to match the directions given by the 2 pairs of corner points
2. a translation $T_{GG'}$ to match the centroids G and G' of the 2 pairs of corner points
3. a scaling S_R to match the length of the line segments defined by the 2 pairs of corner points

Finally, the LV endocardial apex is used to define a scaling S_H along the axis of the heart to match the 2 pairs of axial planes: the valve plane and the one containing the LV endocardial apex.

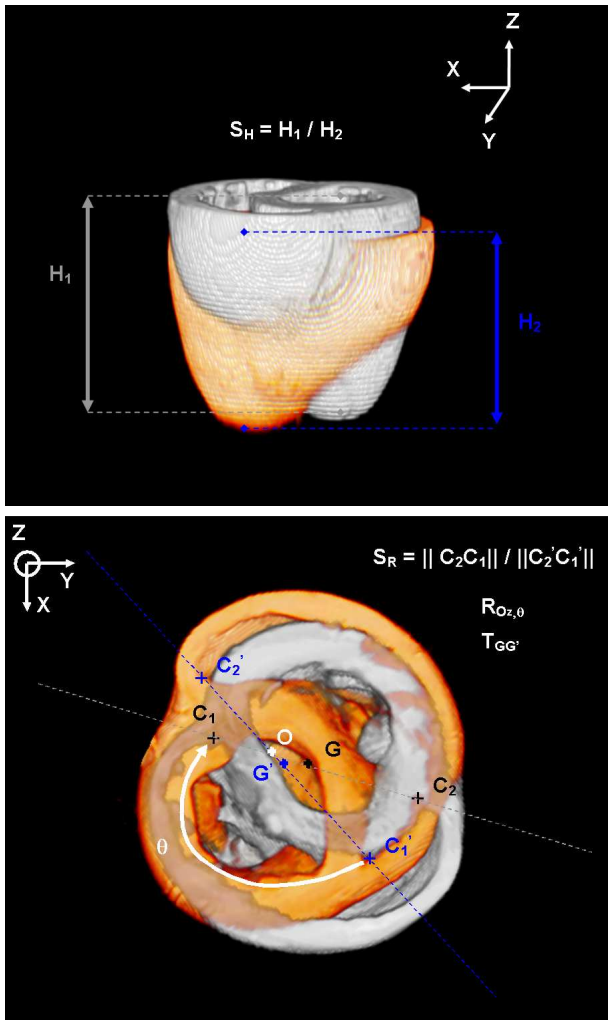

Figure 9: Initialization of the myocardium registration: scaling S_H along the axis of the heart.

A.2 Additional Figures

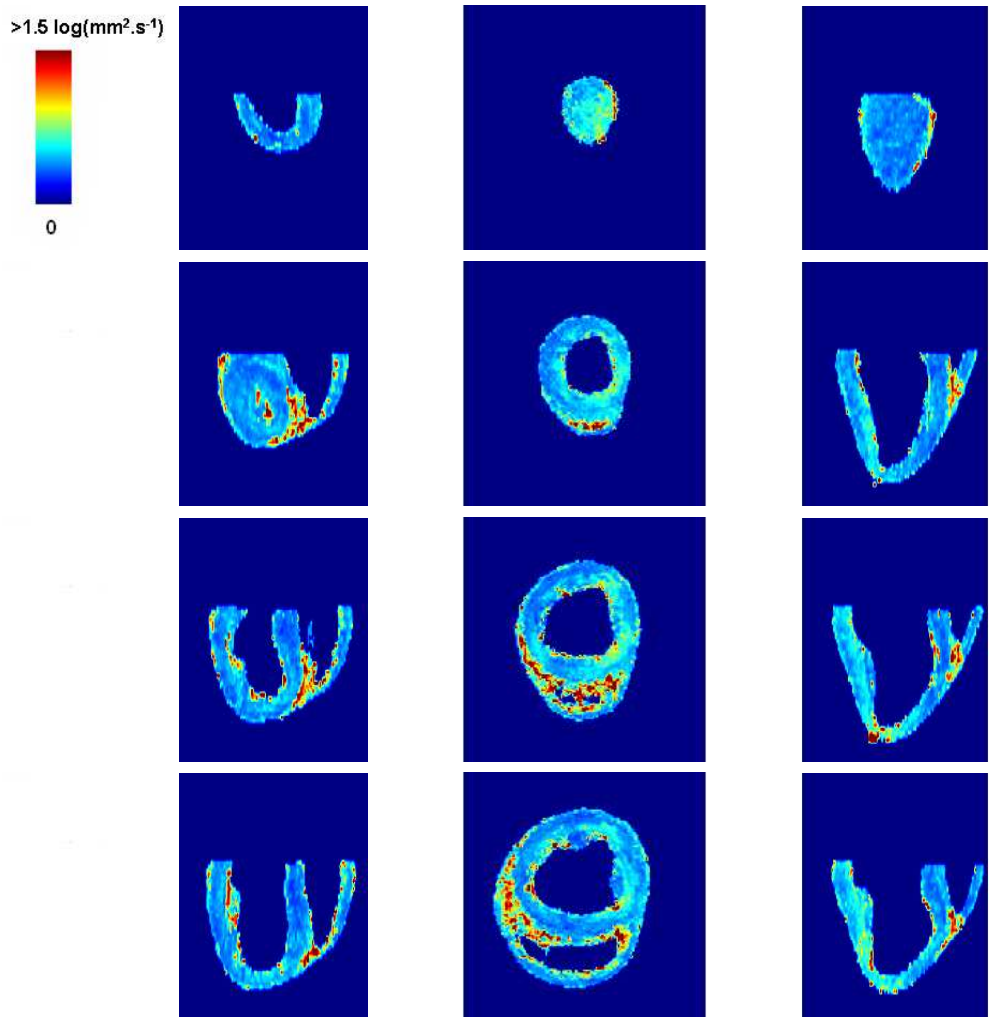

Figure 10: Norm of the covariance matrix in 3 orthogonal views (1/2).

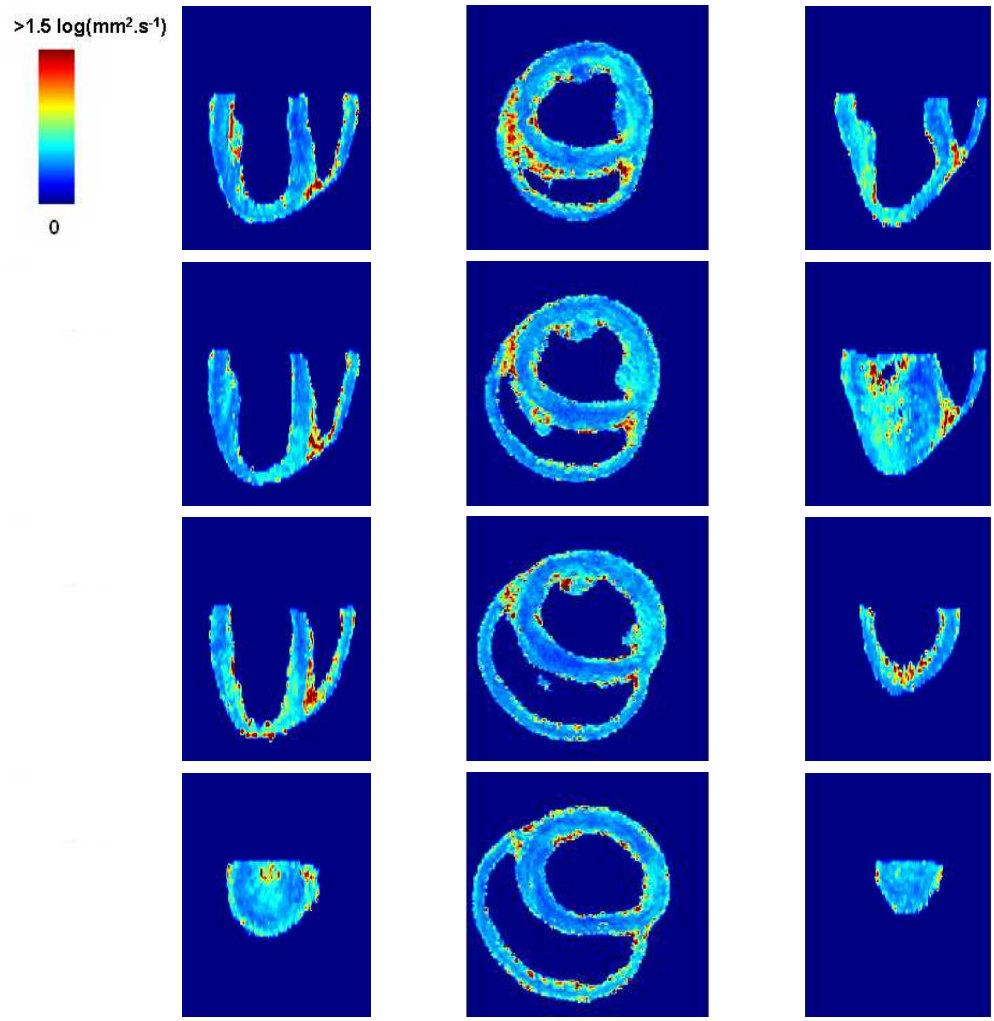

Figure 11: Norm of the covariance matrix in 3 orthogonal views (2/2).

References

[1] D.C. Alexander, C. Pierpaoli, P.J. Basser, and J.C. Gee. Spatial Transformations of Diffusion Tensor Magnetic Resonance Images. *IEEE Transactions on Medical Imaging*, 20(11):1131–1139, 2001.

[2] V. Arsigny, P. Fillard, X. Pennec, and N. Ayache. Fast and Simple Calculus on Tensors in the Log-Euclidean Framework. In *Proceedings of MICCAI'05*, volume LNCS 3749, pages 115–122, 2005.

[3] T. Arts, K.D. Costa, J.W. Covell, and A.D. McCulloch. Relating Myocardial Laminar Architecture to Shear Strain and Muscle Fiber Orientation. *American Journal of Physiology - Heart and Circulatory Physiology*, 280:H2222–H2229, 2001.

[4] N. Ayache, editor. *Computational Models for the Human Body.* Handbook of Numerical Analysis. Elsevier, 2004.

[5] A. Azar, C. Xu, X. Pennec, and N. Ayache. An interactive Intensity- and Feature-Based Non-Rigid Registration Framework for 3D Medical Images. In *Proceedings of ISBI'06*, 2006.

[6] P.J. Basser and S. Pajevic. Statistical Artifacts in Diffusion Tensor MRI (DT-MRI) caused by Background Noise. *Magn. Reson. Med.*, 44(1):41–50, 2000.

[7] Y. Cao, M.I. Miller, R.L. Winslow, and L. Younes. Large Deformation Diffeomorphic Metric Mapping of Fiber Orientations. In *Proceedings of ICCV'05*, pages 1379–1386, 2005.

[8] S. Granger and X. Pennec. Statistiques exactes et approchées sur les normales aléatoires. Research report RR-4533, INRIA, 2002.

[9] A. Guimond, C.R.G. Guttmann, S.K. Warfield, and C.-F. Westin. Deformable registration of DT-MRI data based on transformation invariant tensor characteristics. In *Proceedings of the IEEE International Symposium on Biomedical Imaging (ISBI'02)*, Washington (DC), USA, July 7–10 2002.

[10] K.B. Harrington, F. Rodriguez, A. Cheng, F. Langer, H. Ashikaga, G.T. Daughters, J.C. Criscione, N.B. Ingels, and D.C. Miller. Direct measurement of transmural laminar architecture in the anterolateral wall of the ovine left ventricle: new implications for wall thickening mechanics. *American Journal of Physiology - Heart and Circulatory Physiology*, 1995.

[11] P. Helm. *A Novel Technique for Quantifying Variability of Cardiac Anatomy: Application to the Dyssynchronous Failing Heart.* PhD thesis, Johns Hopkins University, 2005.

[12] P. Helm, M. Faisal Beg, M.I. Miller, and R.L. Winslow. Measuring and mapping cardiac fiber and laminar architecture using diffusion tensor MR imaging. *Ann N Y Acad Sci*, 1047:296–307, Jun 2005.

[13] E.W. Hsu, A.L. Muzikant, S.A. Matulevicius, R.C. Penland, and C.S. Henriquez. Magnetic Resonance Myocardial Fiber-Orientation Mapping with Direct Histological Correlation. *American Journal of Physiology - Heart and Circulatory Physiology*, 274:H1627–H1634, 1998.

[14] D.K. Jones, L.D. Griffin, D.C. Alexander, M. Catanie, M.A. Horsfield, R. Howarda, and S.C.R. Williams. Spatial normalization and Averaging of Diffusion Tensor MRI Data Sets. *NeuroImage*, 17:592–617, 2002.

[15] M.L.G. Joy. MR Current Density and Conductivity Imaging: The state of the art. In *Proceedings EMBS, San Francisco, USA*, 2004.

[16] I.J. LeGrice, B.H. Smaill, L.Z. Chai, S.G. Edgar, J.B. Gavin, and P.J. Hunter. Laminar structure of the heart: ventricular myocyte arrangement and connective tissue architecture in the dog. *American Journal of Physiology - Heart and Circulatory Physiology*, 1995.

[17] X. Pennec, P. Fillard, and N. Ayache. A Riemannian Framework for Tensor Computing. *International Journal of Computer Vision*, 2006.

[18] J. Ruiz-Alzola, C.-F. Westin, S.K. Warfield, C. Alberola, S. Maier, and R. Kikinis. Non-Rigid Registration of 3D Tensor Medical Data. *Med Image Anal*, 6(2):143–61, June 2002.

[19] F. Sachse, editor. *Computational Cardiology - Modeling of Anatomy, Electrophysiology, and Mechanics.* Lecture Notes in Computer Science. Springer, 2004.

[20] D.F. Scollan. *Reconstructing the Heart: Development and Application of Biophysically-based Electrical Models of Propagation in Ventricular Myocardium Reconstructed from Diffusion Tensor MRI.* PhD thesis, Johns Hopkins University, 2002.

[21] D.F. Scollan, A. Holmes, R.L. Winslow, and J. Forder. Histological validation of myocardial microstructure obtained from diffusion tensor magnetic resonance imaging. *American Journal of Physiology - Heart and Circulatory Physiology*, 275:H2308–H2318, 1998.

[22] M. Sermesant, K. Rhode, G.I. Sanchez-Ortiz, O. Camara, R. Andriantsimiavona, S. Hegde, D. Rueckert, P. Lambiase, C. Bucknall, E. Rosenthal, H. Delingette, D.L. Hill, N. Ayache, and R. Razavi. Simulation of cardiac pathologies using an electromechanical biventricular model and XMR interventional imaging. *Med. Image Anal.*, 5(9):467–80, October 2005.

[23] K. Turkowski. *Graphics Gems*, chapter Properties of Surface-Normal Transformations. Academic Press, Inc., 1990.

[24] H. Zhang, P.A. Yushkevich, and J.C. Gee. Registration of Diffusion Tensor Images. In *Proceedings of CVPR'04*, volume 1, pages 842–847, 2004.

Unité de recherche INRIA Sophia Antipolis
2004, route des Lucioles - BP 93 - 06902 Sophia Antipolis Cedex (France)

Unité de recherche INRIA Futurs : Parc Club Orsay Université - ZAC des Vignes
4, rue Jacques Monod - 91893 ORSAY Cedex (France)
Unité de recherche INRIA Lorraine : LORIA, Technopôle de Nancy-Brabois - Campus scientifique
615, rue du Jardin Botanique - BP 101 - 54602 Villers-lès-Nancy Cedex (France)
Unité de recherche INRIA Rennes : IRISA, Campus universitaire de Beaulieu - 35042 Rennes Cedex (France)
Unité de recherche INRIA Rhône-Alpes : 655, avenue de l'Europe - 38334 Montbonnot Saint-Ismier (France)
Unité de recherche INRIA Rocquencourt : Domaine de Voluceau - Rocquencourt - BP 105 - 78153 Le Chesnay Cedex (France)

Éditeur
INRIA - Domaine de Voluceau - Rocquencourt, BP 105 - 78153 Le Chesnay Cedex (France)
http://www.inria.fr
ISSN 0249-6399